Acta Materialia 290 (2025) 120946

Contents lists available at ScienceDirect

Acta Materialia

journal homepage: www.elsevier.com/locate/actamat

Solute clustering in polycrystals: Unveiling the interplay of grain boundary junction and long-range solute attraction effects

Tara Nenninger [a], Frederic Sansoz [a,b,*]

[a] Department of Mechanical Engineering, The University of Vermont, Burlington, VT 05405, USA
[b] Materials Science Program, The University of Vermont, Burlington, VT 05405, USA

ARTICLE INFO

Keywords:
Grain-boundary segregation
Solute clustering
Solute attraction
Grain-boundary junction

ABSTRACT

Spectral analysis of local atomic environments has become a powerful tool for studying solute atom segregation and interactions at grain boundaries in nanocrystalline alloys. When applied to individual grain boundaries, the spectral analysis has shown that solute-solute interaction can be either attractive or repulsive, with long-range relative attraction enhancing the likelihood for solute atoms to begin clustering. In this article, we combine this analysis with a new grain-boundary structure descriptor based on grain-boundary atom coordination, to investigate the impact of grain-boundary junctions on solute atom segregation in polycrystals. Specifically, we systematically characterize the tendency of solute clusters to begin forming at various types of ordinary grain boundaries, triple junctions, and high-order junctions in Ag polycrystals containing either Ni or Cu solute atoms. Our findings demonstrate that the formation of solute clusters at grain boundaries is primarily driven by long-range relative solute attraction, rather than short-range solute-solute interactions. This effect is most pronounced near grain-boundary junctions. Our study highlights the multiscale nature of solute segregation at crystalline interfaces and provides new insights into the complex phenomena governing heterogeneous solute segregation in grain-boundary networks.

1. Introduction

Nanocrystalline (NC) materials are thermodynamically unstable due to their ultrahigh grain boundary (GB) volume fraction [1–3]. This instability arises from the fact that GB atoms possess significantly higher energies than bulk atoms because of their disordered structure. Consequently, grain coarsening occurs to reduce this excess GB energy, which has proven to have detrimental effects on mechanical properties [4]. A successful design strategy for stabilizing nanograins is by engineering NC alloys with a solute that can favorably segregate to the GBs to either lower their energy or pin their movement, while strengthening them at the same time [5–16]. A modern analysis for studying local effects on GB solute segregation in polycrystals is through the lens of GB segregation energy spectra [17–20]. These spectra are produced by atomistic computer simulations using diverse techniques such as density-functional theory [21], semi-empirical-potential-based molecular statics [22,23], or machine learning [24–26]. In those atomistic models, the segregation energy of a solute atom A at a GB atom site i is computed by the equation [25]:

$$\Delta E_i^{seg(A)} = E_{gb,i}^{solute\ A} - E_c^{solute\ A} \tag{1}$$

where $E_{gb,i}^{solute\ A}$ represents the total energy of a polycrystal containing a single solute A at GB atom site i and $E_c^{solute\ A}$ is that with the same solute atom at a different position in the bulk crystal, sufficiently far away from GBs. As such, a negative $\Delta E_i^{seg(A)}$ value indicates favorable segregation of solute A to this specific GB atom site. When applied across all GB atom sites in a polycrystal, a spectrum of GB segregation energies can be established for a given alloy. This approach assumes dilute solute atoms, meaning that no interactions are considered between the solutes.

An important unresolved challenge is predicting the equilibrium GB segregation when solute concentrations exceed their dilute limit and solute-solute interactions become significant [6,23]. Until recently, solute interaction effects in NC alloys have been observed through two distinct behaviors of heterogeneous solute segregation. The first behavior involves a uniform distribution of few-atoms solute clusters within GBs, akin to short-range ordering [27–29]. The second behavior includes heterogeneous segregation of solute among GBs, resulting in either nanoscale solute clusters at GB junctions [29–36] or highly

* Corresponding author.
E-mail address: frederic.sansoz@uvm.edu (F. Sansoz).

https://doi.org/10.1016/j.actamat.2025.120946
Received 14 November 2024; Received in revised form 10 March 2025; Accepted 16 March 2025
Available online 21 March 2025

uneven solute concentrations within different interfaces of the same polycrystal [37–40]. Current segregation models lack the predictive capability to attribute these segregation behaviors to either microstructural features, such as GB junctions, or the inherent attraction of GB solute interactions. In particular, it is observed that GB junctions exhibit different local excess energies and long-range strain or stress fields than flat GBs [41,42], which could arguably influence solute segregation [43,44].

In our previous study on individual symmetric tilt GBs [45], we developed an atomistic algorithm based on spectral analysis of local atomic environments, which revealed distinct short-range and long-range solute-solute interaction energies within single GBs. Other atomistic simulation studies [46–48] have also employed spectral analysis to examine solute-solute interactions at GBs in various alloy polycrystals, though these studies primarily considered only first-neighbor interactions. In our approach, a mean-field method is applied to incorporate long-range interaction effects by averaging solute-solute interaction energies over a group of atoms that extends beyond their closest neighbors. The interaction energy between a solute atom A located at a GB atom site *i* and a neighboring solute atom B fixed at a different GB site is defined as:

$$\Delta E_i^{int} = \Delta E_i^{seg(A+B)} - \Delta E_i^{seg(A)} \tag{2}$$

where $\Delta E_i^{seg(A+B)}$ represents the GB segregation energy of solute A at GB atomic site i in the presence of a second solute atom B at a GB site different from GB site i. By this definition, a negative ΔE_i^{int} value indicates a solute-solute attraction, and repulsion when ΔE_i^{int} is positive. It is hypothesized that the ability to divide GB solute attractions into both short-range and long-range effects is critically important for distinguishing the different types of solute clustering behavior in NC alloys.

In this article, we combine the spectral analysis with a new GB structure descriptor, which is based on GB atom coordination, to investigate the influence of GB junctions on solute atom segregation in Ag polycrystals containing two types of segregating solutes, Cu and Ni. The interatomic potentials used to simulate these two solute elements in Ag polycrystals are expected to show opposite trends in terms of GB solute interactions in single GBs, repulsive for Cu and strongly attractive for Ni [45]. Additionally, hybrid Monte-Carlo and molecular dynamics (MC/MD) simulations are performed to predict the equilibrium segregation behavior in the same Ag polycrystal containing either 4 at.% Cu or 4 at.% Ni solutes. As a result, we systematically characterize the tendency for solute clusters to form at different types of ordinary GBs, triple junctions, and high-order junctions, and test these tendencies with two very distinct solute-solute attraction behaviors.

2. Methodology

2.1. Polycrystal model

A polycrystal was created with the software Atomsk [49] as a cube of side 30 nm with six randomly oriented and randomly distributed grains in pure Ag constructed by Voronoi tessellation scheme. The model had periodic boundary conditions on all sides. The total energy of the structure was minimized by conjugate gradient method with energy (eV) and force (eV/Å) tolerance stopping criteria of 10^{-8} and maximum evaluations set to 10^3 evaluations. Subsequently, a thermal annealing was applied using a Nose-Hoover thermostat and a Parrinello-Rahman barostat held at 500 K and zero pressure for 50 ps. The timestep was 1 fs. Then, the structure was cooled to 1 K at zero pressure over 40 ps in accordance with the methods shown by Wagih et al. [25]. The final polycrystal configuration had a GB atom fraction of 9.1 %, with a total of 1,578,562 atoms. The largest grain was made of 19.9 % of all atoms, and the smallest one, 12.6 %. The average grain size after thermal relaxation was 21 nm. We note that Wagih and Schuh [22] have proven that the GB misorientation angle distribution is random in polycrystals made by the same method. By inspecting our models in the atomistic visualization software OVITO [50], we found that our polycrystals contained mostly high-angle general GBs. Therefore, the GB structure of the simulated polycrystals was considered random in the present study.

2.2. GB atom coordination

To distinguish atoms associated with ordinary GBs, GB triple junctions, or high-order GB junctions in a polycrystal, we developed the *GB atom coordination*, which defines the number of interfaces a GB atom is part of. A Python script was written through the software OVITO [50] to utilize its built-in modifiers. The GB atom coordination was constructed by first identifying each grain in the relaxed pure Ag polycrystal using the Polyhedral Template Matching analysis with an RMSD cutoff of 0 and 'Lattice orientation' chosen as the output. Next, the Grain Segmentation modifier was applied using the automatic Graph Clustering algorithm, with the minimum grain size set to 500 atoms and the 'adopt orphan atoms' and 'handle coherent interphases/stacking' options selected. This identified the six grains in the polycrystal and assigned each of the atoms in the model a new 'grain' attribute numbered from 1 to 6, as can be seen in Fig. 1(a). Additionally, all potential GB segregation sites were given a grain attribute of 0. These sites were chosen as all atoms with a centrosymmetry value greater than or equal to 0.01. As per our previous study [45], the GB segregation sites of interest were not limited to only GB atoms, but also included bulk atoms adjacent to them, as shown in Fig. 1(b).

Second, a volume around each GB atom corresponding to a sphere of influence of 15 Å in radius was isolated. Inside the selected volume, the grain number of the closest neighboring atoms within a 4.5 Å radius was found for each atom. Any unique pair of grain numbers within this smaller radius was denoted as a GB within the sphere of influence. The total number of unique GBs found within the sphere of influence of a GB atom was defined as the GB atom coordination. The final assignment of GB atom coordination for the whole polycrystal can be seen in Fig. 1(c).

Using this metric, a GB coordination of 0 represents an atom in the bulk of a grain. A value of 1 represents an atom in ordinary GB between two grains and a value of 3 a regular GB triple junction. As the number of grains at the junction increases, the total possible number of GBs an atom can be part of increases. For example, considering four grains (A, B, C, and D) that all meet at a high-order junction, there are six possible GBs that an atom in the center of the junction would belong to in this scenario: the AB, AC, AD, BC, BD, and CD boundaries, hence a GB atom coordination of value 6. Now considering a polycrystalline structure with four grains (E, F, G, and H) where the junction is slightly disjointed, like two triple junctions (grains EFG and FGH) that are very close together. In this scenario, there are five, not six, total possible GBs that an atom could be contained within: the EF, EG, FG, FH boundary, and GH boundaries. Due to the random nature of polycrystalline structures, we accounted for this possibility in our GB atom coordination algorithm.

2.3. Local atomic interaction analysis

A generalized form of the embedded-atom-method (EAM) potential based on Finnis-Sinclair formalism was used to compute each pair interaction in Ag-Ni [38], which was fitted on ab-initio calculations to accurately predict the segregation and interaction of Ni solute atoms at GBs in Ag. The Ag-Cu interactions were modeled using an optimized EAM potential by Wu and Trinkle [51]. The size mismatch for the Ag-Ni and Ag-Cu potentials are 15.4 % and 14.6 %, respectively. Past hybrid MC/MD simulations on polycrystals using the same interatomic potentials have predicted that the $Ag_{96}Ni_4$ alloy exhibits heterogeneous Ni segregation in GBs at 500 K [29,35], whereas Cu segregation in the $Ag_{96}Cu_4$ alloy is distributed more homogeneously along GBs at the same temperature [28].

To study short-range and long-range interactions of two GB solutes,

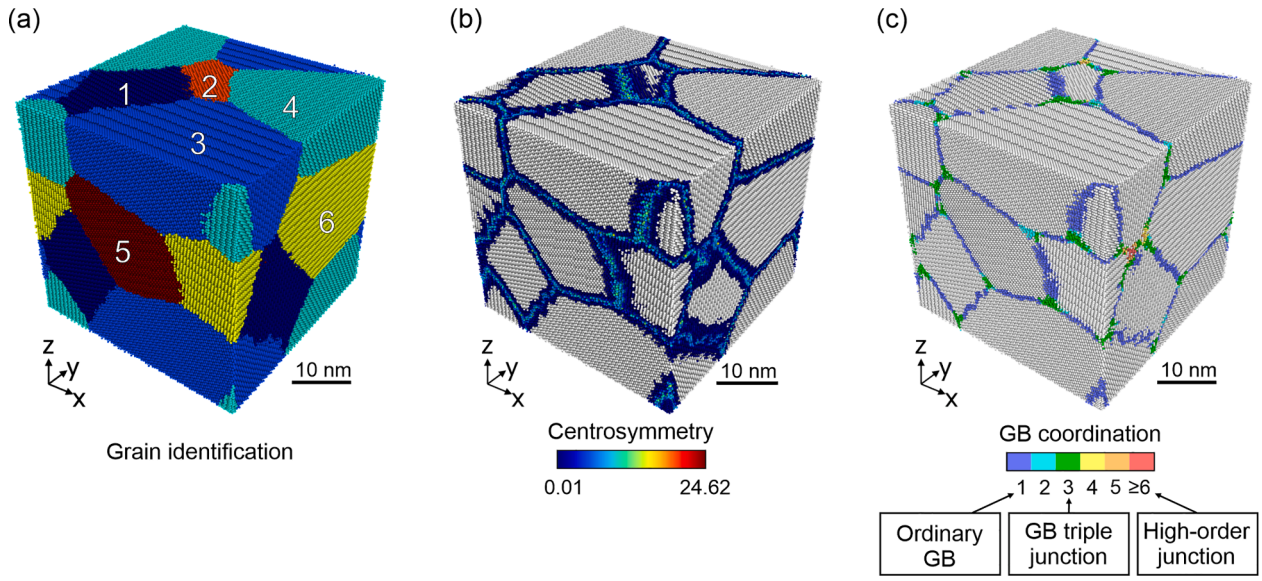

Fig. 1. Relaxed Ag polycrystal with (a) atomic sites highlighted by grain number, (b) heat map of atomic sites with a centro-symmetry parameter greater than 0.01, including GB and GB adjacent sites, and (c) GB sites colored by GB atom coordination. Note that bulk atoms shown in grey color have a GB atom coordination of 0.

we applied the molecular statics (MS) algorithm developed in our previous work [45], which iteratively computes the terms of Eqs. (1) and (2) for each potential GB site. The first step consisted in recording the one-solute segregation energy $\Delta E_i^{seg(A)}$ with each solute A iteratively moved to a different GB site *i* and minimizing the total potential energy. Second, a solute atom B was affixed at a chosen site of interest and the two-solute segregation energy $\Delta E_i^{seg(A+B)}$ was re-calculated with each solute A moved to a different GB site *i*. Third, the solute-solute interaction energy ΔE_i^{int} was calculated as the difference between the one-solute and two-solute segregation energies at each GB site *i*. Fourth, the average solute-solute interaction energy around the fixed solute B was obtained by graphing the radial distance-averaged ΔE_i^{int} for that site. The only change made to the methodology described in [45] corresponds to the selection of the GB site for solute B, which was based on hybrid MC/MD simulation results, instead of GB sites with the highest (most negative) segregation energy. It should be noted that a limitation of this methodology is that it functions solely on the use of atomic substitution as the segregation mechanism. As such, solute diffusion to interstitial sites is ignored as a segregation mechanism due to the nature of the algorithm.

2.4. Segregation simulation using hybrid MC/MD

Hybrid MC/MD simulations were performed in a variance-constrained semi-grand-canonical ensemble at a temperature of 500 K, following the same methodology described in [29]. The variance for MC swap acceptance (κ) was set to 2000. The initial chemical potential difference ($\Delta\mu_0$) was set to 2.0 for the Cu solute and 1.015 for the Ni solute. The MC algorithm was interrupted by short MD runs to achieve both structural relaxation and chemical mixing, which is in accordance with ref [52]. Each MC/MD cycle consisted of trial moves equal to the total number of atoms in the system, followed by 100 MD steps at 500 K. This cycle was repeated 6000 times to reach a total simulation time of 600 ps. Subsequently, each model was cooled down by MD to 1 K at 2 K/ps under zero pressure. The MD timestep was 0.001 ps. MD was performed in the isothermal-isobaric (NPT) ensemble using a Nose-Hoover temperature thermostat and a Parrinello-Rahman barostat fixed at zero pressure in all spatial directions. Since trial rejections occurred at each MC step, differences in concentration and chemical potential were observed. Additionally, to obtain consistent convergence to the target concentration within the total simulation time, the maximum change of chemical potential differences after 10 cycles (i.e. 1000 MD steps) was fixed to 0.1 eV/mol, while the minimum rate of change with respect to the composition difference was fixed at −100 eV/mol for the Cu solute and −10 eV/mol for the Ni solute.

3. Results

3.1. GB site selection from hybrid MC/MD simulations

To investigate local solute interactions in a random polycrystal, we selected two representative GBs based on their equilibrium segregation behavior at a solute concentration of 4 at.%. We performed hybrid MC/MD simulations to study the equilibrium segregation of either Ni or Cu solute atoms in the Ag polycrystal shown in Fig. 1.

At equilibrium (500 K), the Ag – 4 at.% Ni alloy simulation showed that 87.4 % of Ni solute atoms segregated to the GBs. The Ni atoms clustered at GB junctions, and certain GBs were clearly more favorable for Ni segregation based on local solute concentration, as depicted in Fig. 2(a).

In contrast, the simulation for an Ag – 4 at.% Cu alloy indicated that 65 % of Cu solute atoms segregated to the GBs. Unlike the Ni atoms, Cu solute atoms had an even distribution throughout the GB network and no signs of local clustering, as illustrated in Fig. 2(b).

Fig. 3 presents the two GBs selected for more detailed analysis. GB A was an interface exhibiting strong heterogeneous Ni segregation characterized by an uneven Ni solute distribution. At the same time, GB A promoted homogeneous Cu segregation with more uniformly distributed Cu solute atoms across this interface. Additionally, GB B was studied because Ni solute atoms in this interface were found to segregate uniformly rather than heterogeneously, albeit at a high concentration, similarly to an amorphous interface film observed in past experiments in amorphous Ni-Ag alloys [53]. Likewise, GB B exhibited homogeneous Cu segregation with identical uniform Cu solute distribution as in GB A.

The GB atom coordination was computed after each MC/MD simulation to identify any significant structural differences between the two GBs. This analysis was necessary because the two models were generated with different interatomic potentials, resulting in slight variations in their relaxation. Table 1 shows that the overall distribution of atomic sites by GB atom coordination was similar for both GBs. However, significant differences in GB solute concentration were observed between

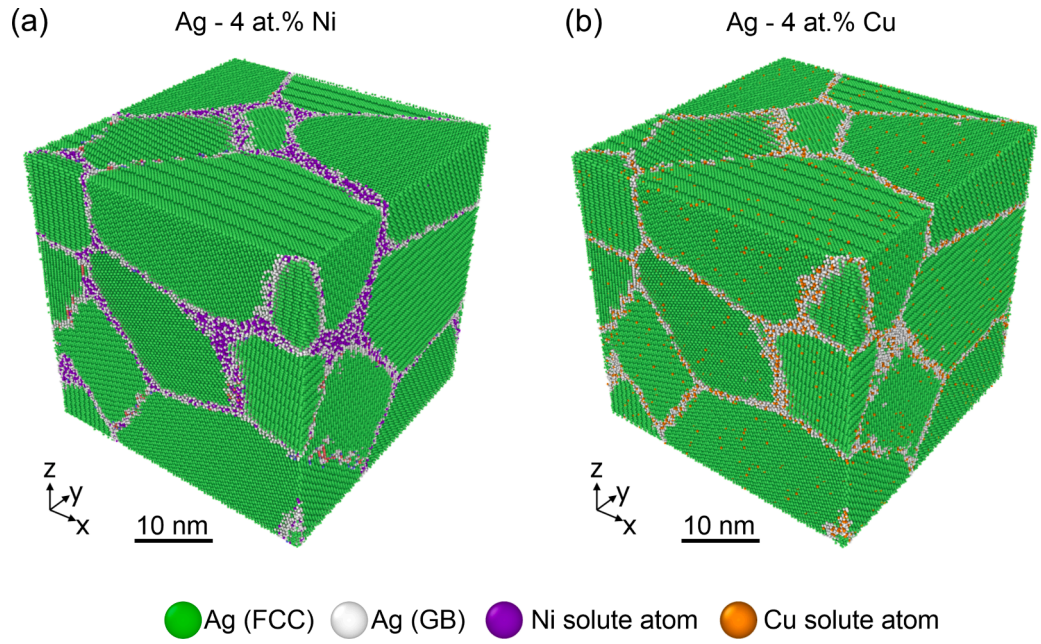

Fig. 2. Hybrid MC/MD simulations of equilibrium segregation states at 500 K in (a) the Ag – 4 at.% Ni alloy and (b) the Ag – 4 at.% Cu alloy.

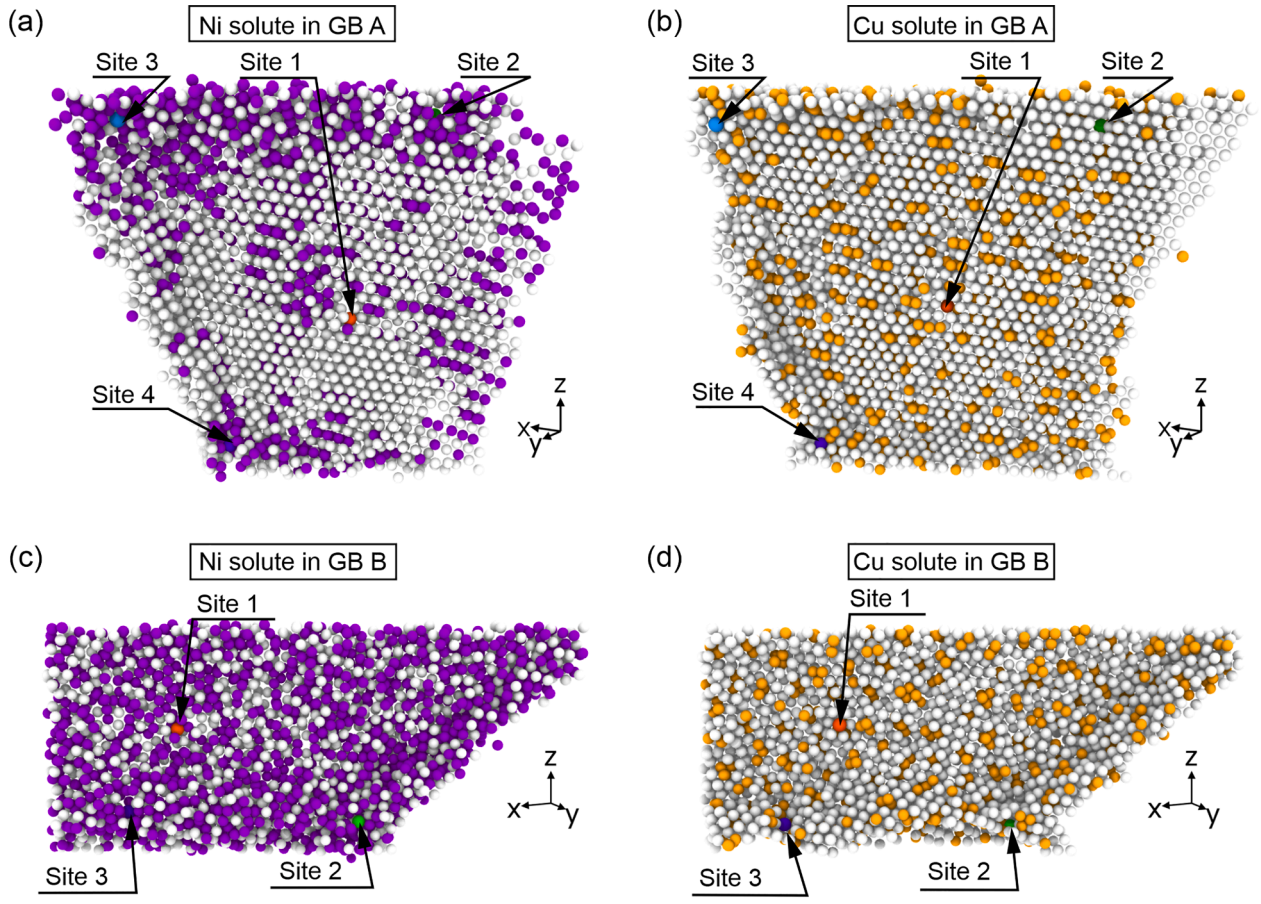

Fig. 3. Hybrid MC/MD simulations with chosen sites of interest indicated on each GB. (a) GB A with Ni solute. (b) GB A with Cu solute. (c) GB B with Ni solute. (d) GB B with Cu solute. Sites 1 and 2 have been highlighted in orange and green colors, respectively, and Sites 3 and 4 in blue color. (For interpretation of the references to colour in this figure legend, the reader is referred to the web version of this article.).

Table 1
The percentage of GB atoms per GB atom coordination number (ACN) in GB A and GB B.

		Ordinary GB	Triple Junction		High-order Junction		
	GB ACN:	1	2	3	4	5	≥ 6
GB A	With Ni Solute	50.30 %	10.13 %	28.44 %	1.08 %	3.08 %	6.25 %
	With Cu Solute	50.69 %	8.42 %	33.17 %	1.33 %	1.67 %	4.72 %
GB B	With Ni Solute	47.41 %	14.46 %	34.88 %	2.47 %	0.78 %	0.00 %
	With Cu Solute	47.33 %	12.19 %	36.80 %	1.79 %	1.88 %	0.00 %

the two solute types. For instance, the average GB solute concentration in GB B was 46.9 % for the Ag – 4 at.% Ni alloy, compared to only 21.3 % for the Ag – 4 at.% Cu alloy. This finding suggests that variations in equilibrium solute segregation are primarily influenced by localized solute-solute attraction effects, prompting the need for spectral analysis at specific GB sites of interest.

We chose representative GB atom sites within GB A and GB B based on their different GB atom coordination numbers, which were either 1, 3, or 6, corresponding to ordinary GBs, GB triple-junctions, or high-order GB junctions, respectively. In GB A, four sites were selected, as shown in Fig. 3(a) and 3(b). Site 1 had a GB atom coordination of 1 (ordinary GB), Site 2 had a GB atom coordination of 3 (GB triple-junction), and Sites 3 and 4 had a GB atom coordination of 6 (high-order junctions). We chose two sites with a GB atom coordination of 6 in GB A for testing, because they were located at opposite corners of the GB, where high-order junctions exhibited varying degrees of clustering in the Ag – 4 at.% Ni alloy after the MC/MD simulation. Site 3 was located inside a large Ni cluster in that simulation, as opposed to Site 4 located in a smaller Ni cluster. In GB B, three sites were selected, as shown in Fig. 3(c) and 3(d). Site 1 had a GB atom coordination of 1 (ordinary GB), Site 2 had a GB coordination of 5 (high-order junction), and Site 3 had a GB coordination of 3 (triple junction).

3.2. Local atomic interaction analysis

3.2.1. Ni solutes in grain boundary A

The spectral analysis of local solute-solute interaction energies with Ni solutes in GB A is shown in Fig. 4(a), along with its local GB atom coordination in Fig. 4(b). Furthermore, Fig. 4(c) presents the graphed radial distance-averaged solute-solute interaction energy (ΔE_{int}) for each test site. Three distinct interaction patterns are observed, corresponding to the GB coordination of each solute site.

At Site 1, which is an ordinary GB site (GB coordination of 1), the averaged ΔE_{int} is positive at all radial distances, indicating solute-solute repulsion, and remains constant at distances above 8 Å. This behavior aligns with the MC/MD results in Fig. 3(a), which show that Site 1 is located in a region of GB A relatively devoid of solute, suggesting a non-segregating site, despite the generally attractive interactions of Ni

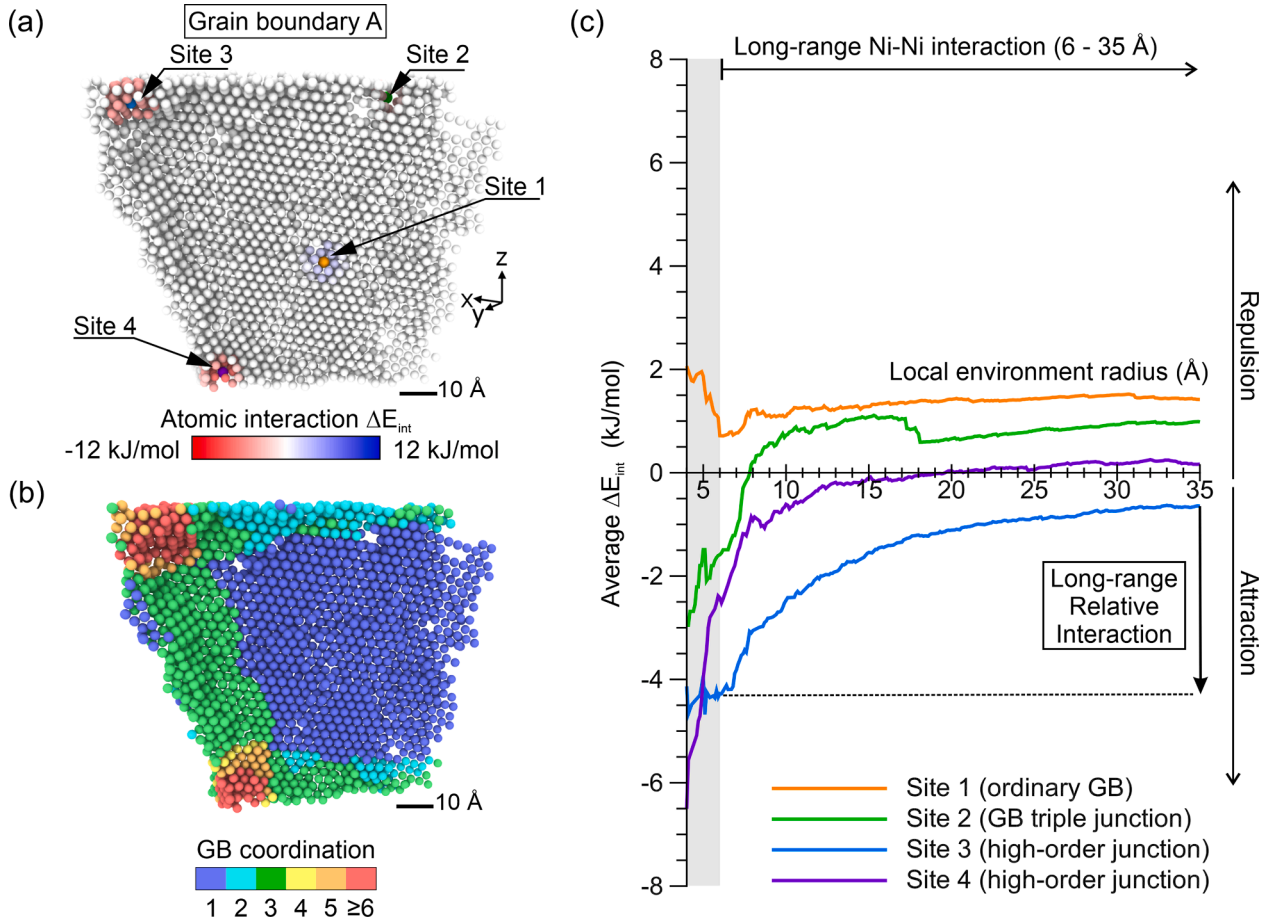

Fig. 4. Spectral analysis of solute-solute interaction energy ΔE_{int} for Ni solute atoms in GB A. (a) Localized heat maps showing ΔE_{int} around Sites 1–4. (b) Atomic sites color-coded by GB atom coordination. (c) Radial distance-averaged energy ΔE_{int} surrounding Sites 1–4. The short-range interaction domain is highlighted in grey and long-range interaction domain is marked by a horizontal arrow. A positive ΔE_{int} indicates repulsive solute-solute interaction, while a negative ΔE_{int} indicates attractive solute-solute interaction. Long-range relative interaction energy is defined as the averaged ΔE_{int} energy taken at a 6Å-radius (short range) minus that at a 35Å-radius (long range), as indicated by the arrow direction in (c).

solutes in Ag [38,45].

At Site 2, which is a triple junction site (GB coordination of 3), the averaged ΔE_{int} is negative at short radial distances but rises sharply to become positive beyond 8 Å, indicating short-range solute-solute attraction but long-range repulsion. In the MC/MD results, Site 2 is located within a large cluster of Ni solute atoms, also part of a triple junction. The short-range attraction observed in Fig. 4(c) directly correlates with the clustering around Site 2 in Fig. 3(a). The long-range increase in average ΔE_{int} reflects a larger radius around Site 2, encompassing both the solute cluster and the central area of GB A, which is void of solute in the MC/MD simulation in Fig. 3(a).

Sites 3 and 4 both are high-order junction sites (GB coordination of 6) but exhibit slightly different behaviors in Fig. 4(c). While both sites show attractive interactions (negative ΔE_{int}) across most radial distances, Site 3 exhibits a more constant average ΔE_{int} in the short range, followed by a steady increase between 7 and 35 Å. In the MC/MD results in Fig. 3(a), Site 3 was found in a large Ni solute cluster at a high-order junction. Notably, the 7 Å range around Site 3 includes all other atomic sites with a GB atom coordination of 6.

Furthermore, as shown in Supplementary Material, a generalization of the above conclusions to the six nearest atom neighbors of Sites 1 and 3, was found.

On the other hand, while Site 4 has also a negative ΔE_{int} over the short range, particularly among its nearest neighbors, ΔE_{int} increases sharply until reaching a radius of 20 Å, where it remains constant through the long range, following the same pattern observed for Site 2 at a triple junction. In the MC/MD results in Fig. 3(a), Site 4 is located inside a smaller Ni cluster at the junction of four grains, surrounded by a solute-devoid area of GB A.

In summary, the spectral analysis of Ni solute segregation in GB A is consistent with the MC/MD simulation results, which predicted highly heterogeneous segregation in this GB. Qualitatively, the tendency for solute clustering can be explained by short-range and long-range interaction behaviors. Here, we define short-range interactions as being significant only for GB sites with first-neighbor atoms, estimated to be approximately 6 Å. Consequently, the domain of long-range interactions spans 6 to 35 Å, as analyzed in Fig. 4(c). Sites with strongly negative average ΔE_{int} at short range align with those predicting larger solute clusters in GB A in the MC/MD simulation. Fig. 4(b) shows that those sites have a greater GB atom coordination as well. This finding suggests that local solute attraction effects increase as GB atom coordination increases.

3.2.2. *Cu solutes in grain boundary A*

The spectral analysis results for Cu solute in GB A, shown in Fig. 5, follow a similar pattern based on GB atom coordination. However, they show significantly different results compared to the Cu solute MC/MD simulation, unlike the Ni solute simulation. The repulsive short-range interactions at Sites 1 (ordinary GB) and 2 (triple junction) align with the MC/MD results in Fig. 3(b), which showed that there was no solute clustering in the Cu solute simulation of GB A. However, in Fig. 5(c), Site 2 displays a negative (attractive) ΔE_{int} at long range, with a significant decrease in ΔE_{int} between 5 and 12 Å, after which it stabilizes through the maximum range of 35 Å. This result indicates strong Cu solute attraction effects near triple junctions. However, no Cu clustering at this site was observed by MC/MD simulation.

Sites 3 and 4 (high-order junction) both exhibit negative (attractive) long-range interactions, but their short-range interactions differ. At Site

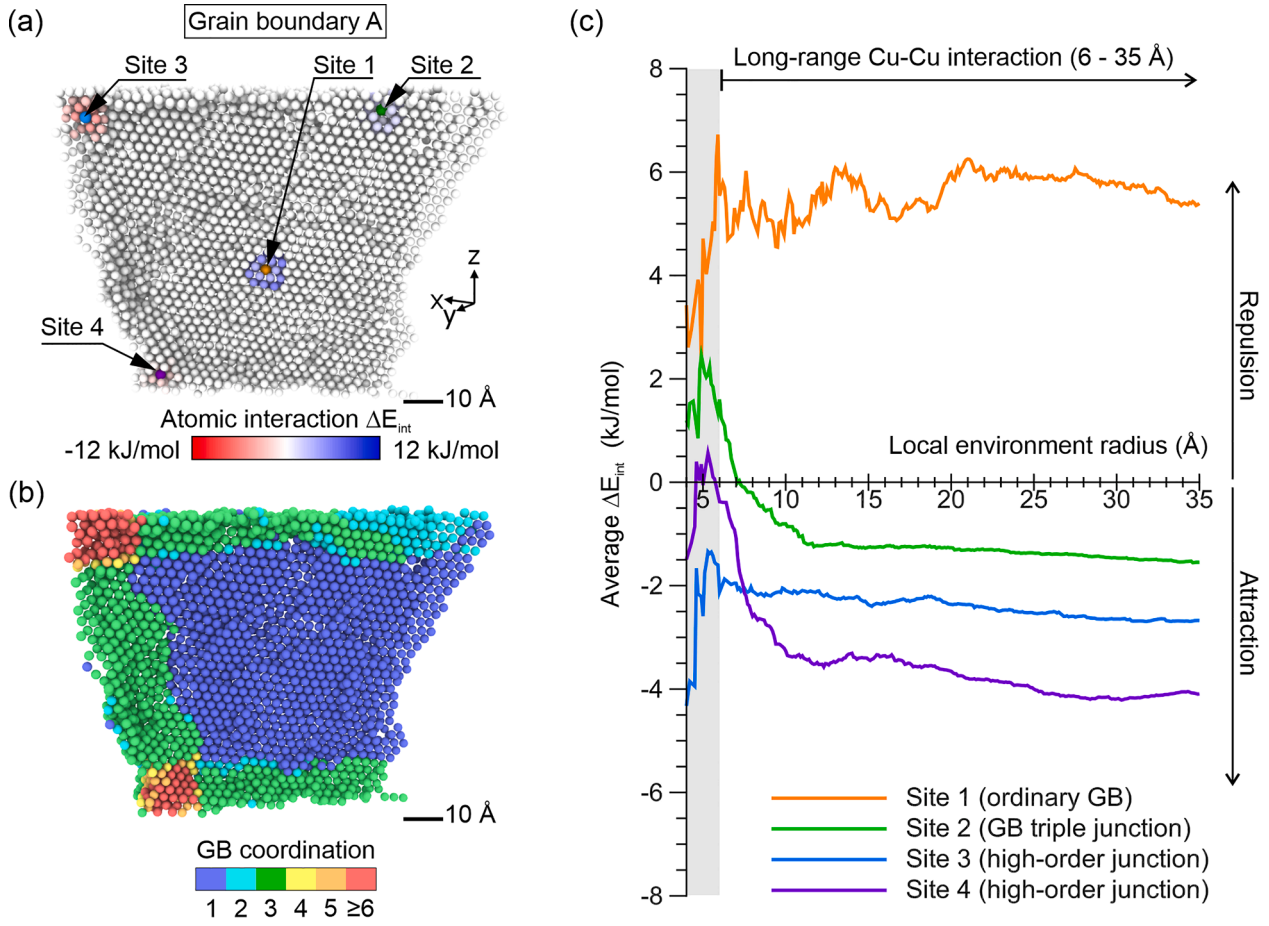

Fig. 5. Spectral analysis of solute-solute interaction energy ΔE_{int} for Cu solute atoms in GB A. (a) Localized heat maps showing ΔE_{int} around Sites 1–4. (b) Atomic sites color-coded by GB atom coordination. (c) Radial distance-averaged energy ΔE_{int} surrounding Sites 1–4.

3, ΔE_{int} is negative and increases sharply within a 6 Å range, then slightly decreases as the radial distance increases. In contrast, at Site 4, ΔE_{int} is higher and increases within the 6 Å range before sharply decreasing over the long range (6 −35 Å). Despite the negative (attractive) ΔE_{int} beyond 6 Å, the absence of clustering in the MC/MD simulation results for both sites, as shown in Fig. 3(b), may be due to the relative increase of ΔE_{int} at short range (6 Å).

The spectral analysis of Cu solute segregation in GB A highlights an important aspect. The MC/MD simulation predicted homogeneous Cu segregation at this interface. However, Fig. 5(c) shows that ΔE_{int} strongly depends on GB atom coordination, ranging from highly positive (repulsive) at the ordinary GB site to strongly negative (attractive) at GB triple junctions and high-order junctions. This analysis suggests that the relative difference between short-range (6 Å) and long-range (up to 35 Å) interaction energies may be a more accurate predictor of solute cluster formation.

We define the *long-range relative interaction energy* as the averaged ΔE_{int} energy taken at a 6Å-radius (short range) minus that at a 35Å-radius (long range), as indicated by the arrow direction in Fig. 4(c). This definition aligns with the sign of ΔE_{int} used throughout this work. The long-range relative interaction energy is positive when the solute-solute interaction becomes more repulsive, as solute A approaches solute B, and negative when the interaction becomes more attractive. It is observed that the long-range relative interaction energy is predominantly positive (repulsive) for Cu solutes across all sites, as indicated in Fig. 5(c), in contrast to the negative (attractive) trend for most sites filled with Ni solutes, as shown in Fig. 4(c). We hypothesize that solute attraction effects are multiscale in nature and are best characterized by long-range relative interaction energies. This hypothesis is further supported by the results for GB B.

3.2.3. Ni solutes in grain boundary B

The spectral analysis results for Ni solutes at three atomic sites in GB B, shown in Fig. 6, are consistent with our previous finding on a symmetric bicrystal in [45], which demonstrated strong solute attraction at all radial distances. In Fig. 6(c), each site exhibits predominantly negative (attractive) solute-solute interactions over both short and long ranges.

Site 1, located at an ordinary GB site (GB coordination of 1), shows the most negative average ΔE_{int} at every radial distance. For Site 2, at a high-order junction (GB coordination of 5), the average ΔE_{int} increases more sharply between 4 and 10 Å, then stabilizes around zero between 10 and 35 Å, indicating minimal influence from solute-solute interactions at these distances. At Site 3, a standard triple junction (GB coordination of 3), the trend of average ΔE_{int} is like that of Site 2 but is shifted towards more negative values.

The strong attractive solute-solute interactions observed for Ni solutes at each site of GB B align with the results from the MC/MD simulation shown in Fig. 3(c) for this interface. In the MC/MD simulation, the strong solute attraction effect was independent of GB atom coordination, leading to the formation of a Ni-rich amorphous interface film, essentially creating one large Ni solute cluster across the entire GB. This behavior is also consistent with the strong long-range relative segregation energies analyzed for each site in Fig. 6(c).

3.2.4. Cu solutes in grain boundary B

The spectral analysis results for Cu solutes in GB B, shown in Fig. 7, reveal similar behaviors across all three sites, which respectively include

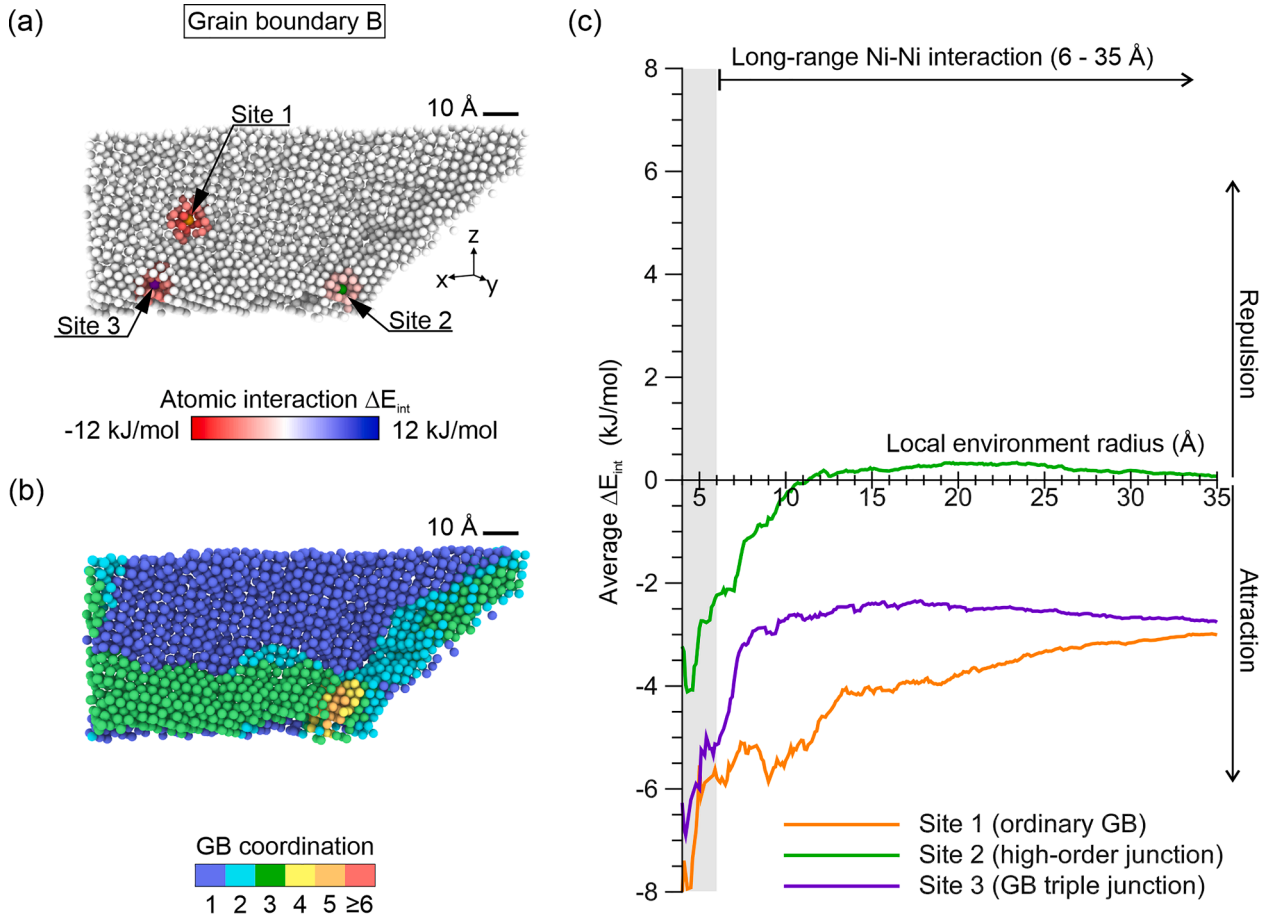

Fig. 6. Spectral analysis of solute-solute interaction energy ΔE_{int} for Ni solute atoms in GB B. (a) Localized heat maps showing ΔE_{int} around Sites 1–3. (b) Atomic sites color-coded by GB atom coordination. (c) Radial distance-averaged energy ΔE_{int} surrounding Sites 1–3.

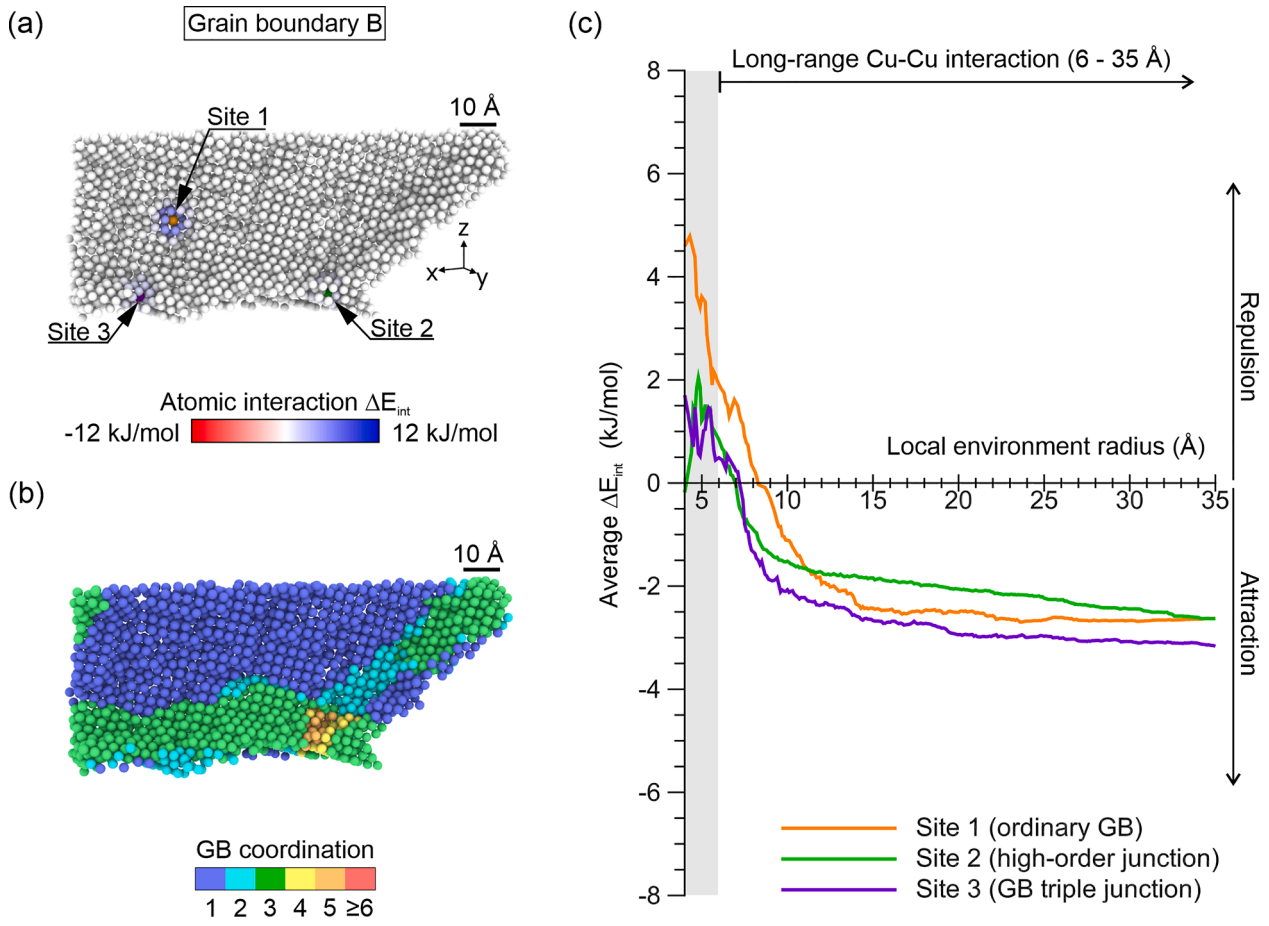

Fig. 7. Spectral analysis of solute-solute interaction energy ΔE_{int} for Cu solute atoms in GB B. (a) Localized heat maps showing ΔE_{int} around Sites 1–3. (b) Atomic sites color-coded by GB atom coordination. (c) Radial distance-averaged energy ΔE_{int} surrounding Sites 1–3.

an ordinary GB, a triple junction and a high-order junction. In Fig. 7(c), the average ΔE_{int} is predominantly positive (repulsive) at short range and negative (attractive) at long range, similarly to our finding for Cu solute at Site 2 in GB A. Despite the long-range solute attraction, the strong repulsive short-range solute-solute interactions observed at each site align with the absence of Cu solute clustering in the MC/MD simulation results shown in Fig. 3(d). Also, the long-range relative interaction energy depicted in Fig. 7(c) is strongly positive (repulsive) across all sites.

4. Discussion

This study used two atomistic modeling techniques to examine GB segregation behavior in polycrystals, specifically at GB junctions. First, hybrid MC/MD simulations were conducted to gain a macroscopic understanding of solute distribution across GB networks at a constant solute concentration. Second, site-specific spectral analysis based on MS simulations was employed to study two-solute interactions, allowing us to quantify short and long-range solute attraction effects on a microscopic scale. Although these two methods offer different perspectives about the evolution of solute clusters at GBs, comparing their results showed that the GB network macrostructure, local solute-solute interactions, and heterogeneous solute segregation behavior are deeply interconnected. This work raises three fundamental questions: What is the role of solute-solute interactions? What is the influence of GB junctions? And how do these factors combine to predict heterogeneity in equilibrium solute segregation in polycrystals? We explore these questions in the following discussion.

4.1. Significance of long-range relative solute interactions

The present findings emphasize the need to consider both short- and long-range solute interaction effects when analyzing the tendency for solute clustering at GBs. In our previous work on solute segregation in symmetric Ag bicrystals, we proposed that a positive average ΔE_{int} indicates repulsion of a secondary solute from a fixed solute, and a negative average ΔE_{int} indicates attraction [45]. This suggested that solute-solute interaction energy could help determine whether solutes are in the initial stages of clustering. However, the current study shows that calculating the long-range relative solute interaction energy may serve as a more accurate predictor for understanding the influence of solute-solute interactions on GB segregation behavior in polycrystals.

To explore this idea further, we compiled the results of our MC/MD simulations and spectral analysis, along with the GB atom coordination computed at each test site, for both solutes in GB A and GB B, as shown in Tables 2 and 3, respectively. These tables provide, for each site, the average ΔE_{int} values at radii of 6 Å and 35 Å, representing the nearest-neighbor and long-range solute-solute interaction energies, respectively. We then calculated the difference between these values, which we defined above as the long-range relative interaction energy. As per our definition, a positive change in this energy is considered as "relative repulsion," while a negative change suggests "relative attraction." Additionally, the tables include the local solute density, predicted at 4 at.% by MC/MD simulations, for a small spherical volume of 6 Å around each test site in the GBs.

GB A was selected as a test boundary because the MC/MD simulations exhibited heterogeneous solute clustering in the Ni solute model, while showing homogeneous segregation behavior in the Cu solute

Table 2
Results across the MC/MD simulations and spectral analysis for both solute types on GB A. GB atoms sites with a high or low local solute density in hybrid MC/MD simulation are highlighted in red and blue colors, respectively.

Solute Type	GB Site	GB Atom Coordination	GB Type	ΔE_{int} at r = 6 Å (kJ/mol)	ΔE_{int} at r = 35 Å (kJ/mol)	Long-Range Relative Interaction (kJ/mol)	MC/MD Local Solute Density within r = 6 Å (atom/nm^3)
Ni Solute	Site 1	1	Ordinary GB	1.134	1.501	-0.367	8.84
	Site 2	3	Triple Junction	-1.587	0.98	-2.567	39.79
	Site 3	6	High-Order Junction	-4.357	-0.653	-3.704	42.00
	Site 4	6	High-Order Junction	-2.634	0.204	-2.838	30.95
Cu Solute	Site 1	1	Ordinary GB	6.727	5.393	1.334	7.74
	Site 2	3	Triple Junction	1.602	-1.546	3.148	12.16
	Site 3	6	High-order Junction	-1.547	-2.675	1.128	9.95
	Site 4	6	High-order Junction	0.103	-4.092	4.195	11.05

Table 3
Results across the MC/MD simulations and spectral analysis for both solute types on GB B. GB atoms sites with a high or low local solute density in hybrid MC/MD simulation are highlighted in red and blue colors, respectively.

Solute Type	GB Site	GB Atom Coordination	GB Type	ΔE_{int} at r = 6 Å (kJ/mol)	ΔE_{int} at r = 35Å (kJ/mol)	Long-Range Relative Interaction (kJ/mol)	MC/MD Local Solute Density within r = 6 Å (atom/nm^3)
Ni Solute	Site 1	1	Ordinary GB	-5.732	-3.001	-2.731	32.05
	Site 2	5	High Order Junction	-2.465	0.078	-2.534	37.58
	Site 3	3	Triple Junction	-5.214	-2.7	-2.514	37.58
Cu Solute	Site 1	1	Ordinary GB	2.16	-2.626	4.786	9.95
	Site 2	5	High Order Junction	1.089	-2.63	3.719	8.84
	Site 3	3	Triple Junction	1.464	-3.168	4.632	11.05

model. Local solute density from the MC/MD simulations was found to be high when it ranged between 30 and 42 atoms/nm^3 and low when it was below 13 atoms/nm^3. Table 2 provides direct evidence that the local solute density was higher and more variable in GB A with Ni solutes compared to Cu solutes.

The spectral analysis for the Ni solute shows that the long-range relative interaction energies at Sites 2, 3, and 4 (representing different types of GB junctions) are strongly negative, indicating a relative attraction. These sites correspond to regions with high solute density in the MC/MD simulations, as highlighted in red in Table 2. In contrast, Site 1 (representing a standard GB) has a low Ni solute density, as highlighted in blue in Table 2. This corresponds well with a near-zero long-range relative solute-solute interaction, combined with a short-range positive (repulsive) interaction with its nearest-neighbor sites.

Now, consider the spectral analysis results for the Cu solute in GB A. All test sites with Cu solutes in Table 2 exhibit long-range relative repulsion, which is consistent with the homogeneous segregation behavior of Cu solutes in the Ag polycrystal, demonstrating resistance to solute clustering even in highly segregating GB structures. Interestingly, however, Site 3, located at a high-order junction, shows negative (attractive) ΔE_{int} in both short- and long-range interactions, unlike the repulsive short-range interactions observed at the other three sites. This finding supports the main conclusion that the tendency of solute clusters to begin forming is primarily driven by long-range relative attraction effects, rather than short-range solute-solute interactions.

Similarly, for GB B, which was selected because MC/MD simulations showed it to be highly saturated with Ni solutes throughout, forming an amorphous thin film, Table 3 shows long-range relative attraction across all sites with Ni solutes (highlighted in red). In contrast, the same boundary displayed homogeneous Cu solute segregation in the Cu solute MC/MD simulation, which matches the long-range relative repulsion observed at the same sites with Cu solutes (highlighted in blue). These

results reinforce the conclusion from GB A that long-range relative attraction or repulsion effects dictate local solute densities inside GBs in polycrystals.

4.2. Atomic elastic stress analysis

To understand how the elastic stress state of the polycrystal was affected by the addition of a single solute atom, we compared the internal von-Mises stress of the polycrystal containing zero solute atoms to that with one solute atom. We used LAMMPS to calculate the virial stress tensor of each atom [54]. Since the virial tensor components are reported in bar•Å^3, we divided these values by the Voronoi atomic volume to compute the Von Mises stress at each atom and converted the result to GPa. This procedure was then repeated with an Ni atom in Site 4 of GB A, and with a Cu atom in the same site of GB A.

Fig. 8(a) shows that the Von Mises stresses σ_{VM} are larger in the GB regions than in the bulk of the grains, suggesting that elastic strain interactions at GBs govern the solute segregation behavior as discussed by Petrazoller et al. [55]. The difference between the one solute stress states and the pure Ag stress state for a Ni or Cu solute at Site 4 in GB A is shown in Fig. 8(b) and (c) respectively, reported as $\Delta\sigma_{VM}$. For Ni solute, the average $\Delta\sigma_{VM}$ was 0.557 GPa within the short-range radius of 6 Å and 0.002 GPa within the long-range radius of 35 Å. For Cu solute, the average $\Delta\sigma_{VM}$ was 0.018 GPa within the short range and −0.002 GPa within the long range. This comparison reveals two distinct elastic stress fields at Site 4, influenced by the type of GB solute, specifically the opposite stress fields found in the long range. This finding confirms that the observed difference in long-range attraction between Ni and Cu solutes at a GB junction could be related to localized GB elastic strain effects in polycrystals.

4.3. Influence of local GB atom coordination

To understand the influence of GB junctions on solute segregation behavior, we examine the relationship between GB atom coordination, spectral analysis, and MC/MD simulation results for GB A. At 4 at.% Ni, the simulation revealed an uneven Ni solute distribution within GB A, with pronounced clustering observed around a triple junction (Site 2) and two high-order junctions with high GB atom coordination (Sites 3 and 4). In contrast, the center of GB A (Site 1) was an ordinary GB relatively devoid of Ni solute, showing no significant clustering. This pattern aligns well with the long-range relative attraction and short-range negative interaction energies observed at Sites 2–4, compared to the short-range positive interaction energy and lack of long-range relative interaction at Site 1, as shown in Fig. 4(c).

This finding establishes a simple criterion: The tendency of solute clusters to begin forming in polycrystals is enhanced by the combined effects of GB junctions and long-range relative attraction. The segregation of Ni solutes in GB A suggests that a macrostructural effect, likely related to GB junctions, influenced the segregation energy and resulted in a Ni-depleted region at Site 1, despite the generally attractive nature of Ni solutes found in a previous study on symmetric Ag bicrystals without GB junctions [45]. The same macrostructural effect appears to intensify the solute attraction at Sites 2–4, as reflected in the solute-solute interaction energies.

The established criterion is further supported by the segregation behavior of Cu solutes in GB A. At 4 at.% Cu, the MC/MD simulation predicted uniform segregation across all sites. However, the spectral analysis shown in Fig. 5(c) suggested a strong dependence of the average ΔE_{int} on GB atom coordination. Site 1 (GB coordination of 1) exhibited strong solute-solute repulsion at all interaction ranges, while Site 2 (coordination of 3) showed a combination of short-range positive interaction energy and long-range relative attraction. Sites 3 and 4 (coordination of 6) displayed both short- and long-range negative ΔE_{int}

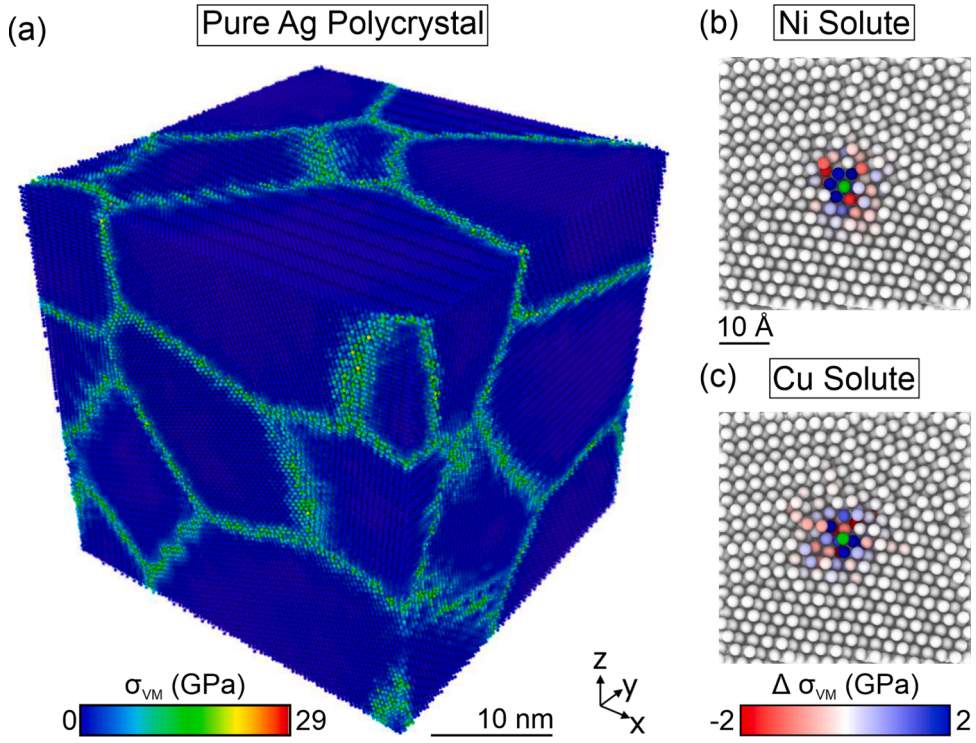

Fig. 8. Atomic Von Mises stress distribution. (a) Von Mises stress in the relaxed pure Ag polycrystal. (b) Change in Von Mises stress between the pure Ag polycrystal and the polycrystal with one Ni solute atom located at Site 4 of GB A, highlighted in green. (c) Change in Von Mises stress between the pure Ag polycrystal and the polycrystal with one Cu solute atom located at Site 4 of GB A, highlighted in green. (For interpretation of the references to colour in this figure legend, the reader is referred to the web version of this article.).

values, indicating a strong attraction to solutes. However, the long-range relative interaction energies are positive (i.e., relative repulsion) for Sites 2–4, preventing the initialization of Cu solute clusters. This case demonstrates that the conditions of GB junction presence and long-range relative attraction are not always met simultaneously, which may explain the absence of Cu clustering in the MC/MD simulation.

Finally, we validate the robustness of this criterion with GB B. As shown in Figs. 6(c) and 7(c), there is no significant influence of GB atom coordination on long-range interactions, either attractive or repulsive, at this interface. In the Ag-4 at.% Ni alloy, the solute forms an amorphous thin film due to long-range attraction across all sites, as predicted by spectral analysis. In contrast, in the Ag-4 at.% Cu alloy, segregation is homogeneous, driven by long-range relative repulsion observed at every site.

Overall, this theory offers new insights into GB junction solute clustering, helping to explain previous experimental observations of higher solute concentrations at triple junctions compared to ordinary GBs [14,36,56]. Because it involves only MS predictions at zero temperature, our methodology reveals that the solute clustering mechanism is driven by a direct attraction toward GB junctions, without the intervention of solute diffusion along the GBs. Therefore, this finding could be critical for improving the accuracy of thermodynamics phase-field models of GB segregation in polycrystals that rely on diffuse interface theories [57–59].

4.4. Predicting solute clustering and heterogeneity

The purpose of this study was primarily to identify the main driving factor behind heterogeneous GB segregation behavior in NC alloys. However, it is essential to clarify that, at this stage, heterogeneous segregation is defined as any behavior that is not homogeneous throughout the entire polycrystal. We investigated two distinct examples of heterogeneous segregation in GB A and GB B. In GB A, our Ag–4 at.% Ni equilibrium MC/MD simulation revealed internally heterogeneous solute clustering, indicating that the locations of these clusters were directly linked to the positions of GB junctions. In contrast, the macrostructural effect that caused GB B to exhibit such significant segregation with Ni solutes, resulting in the formation of an amorphous interface film throughout GB B in this simulation, remains unclear.

A particularly intriguing discovery is that GB junctions with the same GB atom coordination, such as the two high-order junction regions of GB A shown in Fig. 4(c), displayed different cluster sizes of Ni solutes in the same MC/MD simulation. This suggests that while these GB junctions had a high likelihood of solute cluster formation, the evolution of the clusters varied as solute concentration increased. In the case of GB A, we can envision a competition for solute atom attraction among neighboring GB junctions. This effect could amplify the heterogeneous segregation behavior in alloy polycrystals with a high density of junctions, such as NC alloys.

This observation could suggest that long-range relative attraction between two solute atoms may change when one solute interacts with a pre-existing solute cluster. In other words, there could be a cluster size effect on GB junction solute attraction. Another potential reason could be linked to entropic effects on GB junction solute attraction [60], which have been ignored in the present study and would require more complex computations of entropy spectra for GB segregation in polycrystals [61].

5. Conclusion

In conclusion, we find that spectral analysis of short-range and long-range solute-solute interaction energies within GBs in random polycrystals is a highly effective approach for predicting the tendency of solute cluster formation at GB junctions. The most accurate metric for predicting GB solute clustering is the long-range relative solute interaction energy, defined as the difference between the distance-averaged solute-solute interaction energies in the first-neighbor and long-range atomic environments, identified in this study as 6 Å and 35 Å, respectively.

We also introduced the GB atom coordination number as a new descriptor for the GB network macrostructure in polycrystals, particularly for identifying regular triple junctions and high-order GB junctions. By pairing spectral analysis with GB atom coordination, we demonstrate that the tendency of solute clusters to begin forming in polycrystals is enhanced by the combined effects of GB junctions and long-range relative solute attraction. This criterion is validated through hybrid MC/MD simulation results showing heterogeneous GB segregation and solute clustering in Ag polycrystals containing Ni solutes. Conversely, the absence of clustering with Cu solutes in the MC/MD simulations is explained by the lack of simultaneous conditions of GB junction presence and long-range relative solute attraction.

Overall, this study reveals the multiscale nature of solute interactions near GB junctions in polycrystals, without involving solute diffusion along the GBs. These findings may help explain previous experimental observations of higher solute concentrations at triple junctions in NC alloys, compared to ordinary GBs.

CRediT authorship contribution statement

Tara Nenninger: Writing – review & editing, Writing – original draft, Validation, Methodology, Investigation, Formal analysis, Data curation, Conceptualization. **Frederic Sansoz:** Writing – review & editing, Writing – original draft, Supervision, Project administration, Methodology, Funding acquisition, Formal analysis, Conceptualization.

Declaration of competing interest

The authors declare that they have no known competing financial interests or personal relationships that could have appeared to influence the work reported in this paper.

Acknowledgements

This research received support by the U.S. Department of Energy under grant No DE-SC0020054 and used resources of the NERSC, a U.S. Department of Energy Office of Science User Facility located at Lawrence Berkeley National Laboratory, operated under Contract No DE-AC02–05CH11231.

Supplementary materials

Supplementary material associated with this article can be found, in the online version, at doi:10.1016/j.actamat.2025.120946.

References

[1] C.C. Koch, R.O. Scattergood, M. Saber, H. Kotan, High temperature stabilization of nanocrystalline grain size: thermodynamic versus kinetic strategies, J. Mater. Res. 28 (13) (2013) 1785–1791, https://doi.org/10.1557/jmr.2012.429.
[2] A.R. Kalidindi, T. Chookajorn, C.A. Schuh, Nanocrystalline materials at Equilibrium: a thermodynamic review, JOM 67 (12) (2015) 2834–2843, https://doi.org/10.1007/s11837-015-1636-9.
[3] Y. Zou, J.M. Wheeler, H. Ma, P. Okle, R. Spolenak, Nanocrystalline high-entropy alloys: a new paradigm in high-temperature strength and stability, Nano Lett. 17 (3) (2017) 1569–1574, https://doi.org/10.1021/acs.nanolett.6b04716.
[4] D.S. Gianola, S. Van Petegem, M. Legros, S. Brandstetter, H. Van Swygenhoven, K. J. Hemker, Stress-assisted discontinuous grain growth and its effect on the deformation behavior of nanocrystalline aluminum thin films, Acta Mater. 54 (8) (2006) 2253–2263, https://doi.org/10.1016/j.actamat.2006.01.023.
[5] D.L. Beke, C. Cserháti, I.A. Szabó, Segregation inhibited grain coarsening in nanocrystalline alloys, J. Appl. Phys. 95 (9) (2004) 4996–5001, https://doi.org/10.1063/1.1688461. %J Journal of Applied Physics.
[6] A.J. Detor, C.A. Schuh, Grain boundary segregation, chemical ordering and stability of nanocrystalline alloys: atomistic computer simulations in the Ni–W system, Acta Mater. 55 (12) (2007) 4221–4232, https://doi.org/10.1016/j.actamat.2007.03.024.

[7] K.A. Darling, R.N. Chan, P.Z. Wong, J.E. Semones, R.O. Scattergood, C.C. Koch, Grain-size stabilization in nanocrystalline FeZr alloys, Scr. Mater. 59 (5) (2008) 530–533, https://doi.org/10.1016/j.scriptamat.2008.04.045.

[8] K.A. Darling, B.K. VanLeeuwen, C.C. Koch, R.O. Scattergood, Thermal stability of nanocrystalline Fe–Zr alloys, Mater. Sci. Eng.: A 527 (15) (2010) 3572–3580, https://doi.org/10.1016/j.msea.2010.02.043.

[9] D. Raabe, M. Herbig, S. Sandlöbes, Y. Li, D. Tytko, M. Kuzmina, D. Ponge, P. P. Choi, Grain boundary segregation engineering in metallic alloys: a pathway to the design of interfaces, Curr. Opin. Solid State Mater. Sci. 18 (4) (2014) 253–261, https://doi.org/10.1016/j.cossms.2014.06.002.

[10] T. Chookajorn, C.A. Schuh, Nanoscale segregation behavior and high-temperature stability of nanocrystalline W–20at.% Ti, Acta Mater. 73 (2014) 128–138, https://doi.org/10.1016/j.actamat.2014.03.039.

[11] S.J.B. Kurz, A. Leineweber, E.J. Mittemeijer, Anomalously high density and thermal stability of nanotwins in Ni(W) thin films: quantitative analysis by x-ray diffraction, J. Mater. Res. 29 (15) (2014) 1642–1655, https://doi.org/10.1557/jmr.2014.202.

[12] T. Chookajorn, M. Park, C.A. Schuh, Duplex nanocrystalline alloys: entropic nanostructure stabilization and a case study on W–Cr, J. Mater. Res. 30 (2) (2015) 151–163, https://doi.org/10.1557/jmr.2014.385.

[13] A. Khalajhedayati, T.J. Rupert, High-temperature stability and grain boundary complexion formation in a nanocrystalline Cu-Zr alloy, JOM 67 (12) (2015) 2788–2801, https://doi.org/10.1007/s11837-015-1644-9.

[14] B. Färber, E. Cadel, A. Menand, G. Schmitz, R. Kirchheim, Phosphorus segregation in nanocrystalline Ni–3.6 at.% P alloy investigated with the tomographic atom probe (TAP), Acta Mater. 48 (3) (2000) 789–796, https://doi.org/10.1016/S1359-6454(99)00397-3.

[15] R.K. Koju, Y. Mishin, Atomistic study of grain-boundary segregation and grain-boundary diffusion in Al-Mg alloys, Acta Mater. 201 (2020) 596–603, https://doi.org/10.1016/j.actamat.2020.10.029.

[16] K.A. Darling, M. Rajagopalan, M. Komarasamy, M.A. Bhatia, B.C. Hornbuckle, R. S. Mishra, K.N. Solanki, Extreme creep resistance in a microstructurally stable nanocrystalline alloy, Nature 537 (7620) (2016) 378–381, https://doi.org/10.1038/nature19313.

[17] C.L. White, W.A. Coghlan, The spectrum of binding energies approach to grain boundary segregation, Metall. Trans. A 8 (9) (1977) 1403–1412, https://doi.org/10.1007/BF02642853.

[18] C.L. White, D.F. Stein, Sulfur segregation to grain boundaries in Ni3Al and Ni3(AI, Ti) alloys, Metall. Trans. A 9 (1) (1978) 13–22, https://doi.org/10.1007/BF02647165.

[19] T. Mütschele, R. Kirchheim, Segregation and diffusion of hydrogen in grain boundaries of palladium, Scripta Metallurgica 21 (2) (1987) 135–140, https://doi.org/10.1016/0036-9748(87)90423-6.

[20] P. Lejček, S. Hofmann, Thermodynamics and structural aspects of grain boundary segregation, Crit. Rev. Solid State Mater. Sci. 20 (1) (1995) 1–85, https://doi.org/10.1080/10408439508243544.

[21] L. Huber, B. Grabowski, M. Militzer, J. Neugebauer, J. Rottler, Ab initio modelling of solute segregation energies to a general grain boundary, Acta Mater. 132 (2017) 138–148, https://doi.org/10.1016/j.actamat.2017.04.024.

[22] M. Wagih, C.A. Schuh, Spectrum of grain boundary segregation energies in a polycrystal, Acta Mater. 181 (2019) 228–237, https://doi.org/10.1016/j.actamat.2019.09.034.

[23] M. Wagih, C.A. Schuh, Grain boundary segregation beyond the dilute limit: separating the two contributions of site spectrality and solute interactions, Acta Mater. 199 (2020) 63–72, https://doi.org/10.1016/j.actamat.2020.08.022.

[24] L. Huber, R. Hadian, B. Grabowski, J. Neugebauer, A machine learning approach to model solute grain boundary segregation, npj Comput. Mater. 4 (1) (2018) 64, https://doi.org/10.1038/s41524-018-0122-7.

[25] M. Wagih, P.M. Larsen, C.A. Schuh, Learning grain boundary segregation energy spectra in polycrystals, Nat. Commun. 11 (1) (2020) 6376, https://doi.org/10.1038/s41467-020-20083-6.

[26] Y. Mahmood, M. Alghalayini, E. Martinez, C.J.J. Paredis, F. Abdeljawad, Atomistic and machine learning studies of solute segregation in metastable grain boundaries, Sci. Rep. 12 (1) (2022) 6673, https://doi.org/10.1038/s41598-022-10566-5.

[27] Z. Pan, T.J. Rupert, Spatial variation of short-range order in amorphous intergranular complexions, Comput. Mater. Sci. 131 (2017) 62–68, https://doi.org/10.1016/j.commatsci.2017.01.033.

[28] F. Sansoz, X. Ke, Hall-petch strengthening limit through partially active segregation in nanocrystalline Ag-Cu alloys, Acta Mater. 225 (2021) 117560, https://doi.org/10.1016/j.actamat.2021.117560.

[29] E.-A. Picard, F. Sansoz, Ni solute segregation and associated plastic deformation mechanisms into random FCC Ag, BCC Nb and HCP Zr polycrystals, Acta Mater. 240 (2022) 118367, https://doi.org/10.1016/j.actamat.2022.118367.

[30] T. Frolov, K.A. Darling, L.J. Kecskes, Y. Mishin, Stabilization and strengthening of nanocrystalline copper by alloying with tantalum, Acta Mater. 60 (5) (2012) 2158–2168, https://doi.org/10.1016/j.actamat.2012.01.011.

[31] B.C. Hornbuckle, T. Rojhirunsakool, M. Rajagopalan, T. Alam, G.P. Purja Pun, R. Banerjee, K.N. Solanki, Y. Mishin, L.J. Kecskes, K.A. Darling, Effect of Ta solute concentration on the microstructural evolution in immiscible Cu-Ta alloys, JOM 67 (12) (2015) 2802–2809, https://doi.org/10.1007/s11837-015-1643-x.

[32] X. Zhou, X.-x. Yu, T. Kaub, R.L. Martens, G.B. Thompson, Grain boundary specific segregation in nanocrystalline Fe(Cr), Sci. Rep. 6 (1) (2016) 34642, https://doi.org/10.1038/srep34642.

[33] J.D. Schuler, T.J. Rupert, Materials selection rules for amorphous complexion formation in binary metallic alloys, Acta Mater. 140 (2017) 196–205, https://doi.org/10.1016/j.actamat.2017.08.042.

[34] J. Hu, Y.N. Shi, X. Sauvage, G. Sha, K. Lu, Grain boundary stability governs hardening and softening in extremely fine nanograined metals, Science (1979) 355 (6331) (2017) 1292–1296, https://doi.org/10.1126/science.aal5166.

[35] Z. Pan, F. Sansoz, Heterogeneous solute segregation suppresses strain localization in nanocrystalline Ag-Ni alloys, Acta Mater. 200 (2020) 91–100, https://doi.org/10.1016/j.actamat.2020.08.074.

[36] A.K. Barnett, O. Hussein, M. Alghalayini, A. Hinojos, J.E. Nathaniel II, D.L. Medlin, K. Hattar, B.L. Boyce, F. Abdeljawad, Triple junction segregation dominates the stability of nanocrystalline alloys, Nano Lett. 24 (31) (2024) 9627–9634, https://doi.org/10.1021/acs.nanolett.4c02395.

[37] C.J. O'brien, C.M. Barr, P.M. Price, et al., Grain boundary phase transformations in PtAu and relevance to thermal stabilization of bulk nanocrystalline materials, J. Mater. Sci. 53 (2017) 2911–2927, https://doi.org/10.1007/s10853-017-1706-1.

[38] Z. Pan, V. Borovikov, M. Mendelev, F. Sansoz, Development of a semi-empirical potential for simulation of Ni solute segregation into grain boundaries in Ag, modelling and simulation, Mater. Sci. Eng. 26 (2018), https://doi.org/10.1088/1361-651X/aadea3.

[39] C.M. Barr, S.M. Foiles, M. Alkayyali, Y. Mahmood, P.M. Price, D.P. Adams, B. L. Boyce, F. Abdeljawad, K. Hattar, The role of grain boundary character in solute segregation and thermal stability of nanocrystalline Pt–Au, Nanoscale 13 (6) (2021) 3552–3563, https://doi.org/10.1039/D0NR07180C.

[40] X. Zhou, Y. Wei, M. Kühbach, H. Zhao, F. Vogel, R. Darvishi Kamachali, G. B. Thompson, D. Raabe, B. Gault, Revealing in-plane grain boundary composition features through machine learning from atom probe tomography data, Acta Mater. 226 (2022) 117633, https://doi.org/10.1016/j.actamat.2022.117633.

[41] S. Shekhar, A.H. King, Strain fields and energies of grain boundary triple junctions, Acta Mater. 56 (19) (2008) 5728–5736, https://doi.org/10.1016/j.actamat.2008.07.053.

[42] N. Tuchinda, C.A. Schuh, Triple junction excess energy in polycrystalline metals, Acta Mater. 279 (2024) 120274, https://doi.org/10.1016/j.actamat.2024.120274.

[43] N. Tuchinda, C.A. Schuh, Triple junction solute segregation in Al-based polycrystals, Phys. Rev. Mater. 7 (2) (2023) 023601, https://doi.org/10.1103/PhysRevMaterials.7.023601.

[44] M.E. Fernandez, R. Dingreville, D.L. Medlin, D.E. Spearot, The effect of grain boundary facet junctions on segregation and embrittlement, Acta Mater. 269 (2024) 119805, https://doi.org/10.1016/j.actamat.2024.119805.

[45] T. Nenninger, F. Sansoz, Local atomic environment analysis of short and long-range solute-solute interactions in a symmetric tilt grain boundary, Scr. Mater. 222 (2023) 115045, https://doi.org/10.1016/j.scriptamat.2022.115045.

[46] T.P. Matson, C.A. Schuh, Atomistic assessment of solute-solute interactions during grain boundary segregation, Nanomaterials (2021).

[47] T.P. Matson, C.A. Schuh, A "bond-focused" local atomic environment representation for a high throughput solute interaction spectrum analysis, Acta Mater. 278 (2024) 120275, https://doi.org/10.1016/j.actamat.2024.120275.

[48] Z. Zhang, C. Deng, Grain boundary segregation prediction with a dual-solute model, Phys. Rev. Mater. 8 (10) (2024) 103605, https://doi.org/10.1103/PhysRevMaterials.8.103605.

[49] P. Hirel, Atomsk: a tool for manipulating and converting atomic data files, Comput. Phys. Commun. 197 (2015) 212–219, https://doi.org/10.1016/j.cpc.2015.07.012.

[50] A. Stukowski, Visualization and analysis of atomistic simulation data with OVITO–the open visualization tool, Model. Simul. Mat. Sci. Eng. 18 (1) (2010) 015012, https://doi.org/10.1088/0965-0393/18/1/015012.

[51] H.H. Wu, D.R. Trinkle, Cu/Ag EAM potential optimized for heteroepitaxial diffusion from ab initio data, Comput. Mater. Sci. 47 (2) (2009) 577–583, https://doi.org/10.1016/j.commatsci.2009.09.026.

[52] B. Sadigh, P. Erhart, A. Stukowski, A. Caro, E. Martinez, L. Zepeda-Ruiz, Scalable parallel Monte Carlo algorithm for atomistic simulations of precipitation in alloys, Phys. Rev. B 85 (18) (2012) 184203.

[53] J.H. He, H.W. Sheng, P.J. Schilling, C.L. Chien, E. Ma, Amorphous structures in the immiscible Ag-Ni system, Phys. Rev. Lett. 86 (13) (2001) 2826–2829, https://doi.org/10.1103/PhysRevLett.86.2826.

[54] A.P. Thompson, S.J. Plimpton, W. Mattson, General formulation of pressure and stress tensor for arbitrary many-body interaction potentials under periodic boundary conditions, J. Chem. Phys. 131 (15) (2009), https://doi.org/10.1063/1.3245303.

[55] J. Petrazoller, J. Guénolé, S. Berbenni, T. Richeton, On the effect of elastic anisotropy and polarizability on solute segregation at low-angle grain boundaries, Comput. Mater. Sci. 249 (2025) 113642, https://doi.org/10.1016/j.commatsci.2024.113642.

[56] G.F.B. Moladje, S. Das, A. Verma, Y.T. Chang, M.A. Charpagne, R.S. Averback, P. Bellon, Grain boundary precipitation and self-organization in two-phase alloys under irradiation: phase field simulations and experiments in Al-Sb, JOM 76 (6) (2024) 2884–2898, https://doi.org/10.1007/s11837-024-06503-8.

[57] F. Abdeljawad, S.M. Foiles, Stabilization of nanocrystalline alloys via grain boundary segregation: a diffuse interface model, Acta Mater. 101 (2015) 159–171, https://doi.org/10.1016/j.actamat.2015.07.058.

[58] F. Abdeljawad, P. Lu, N. Argibay, B.G. Clark, B.L. Boyce, S.M. Foiles, Grain boundary segregation in immiscible nanocrystalline alloys, Acta Mater. 126 (2017) 528–539, https://doi.org/10.1016/j.actamat.2016.12.036.

[59] O. Hussein, Y. Mishin, A model of thermodynamic stabilization of nanocrystalline grain boundaries in alloy systems, Acta Mater. 281 (2024) 120404, https://doi.org/10.1016/j.actamat.2024.120404.
[60] P. Lejček, S. Hofmann, M. Všianská, M. Šob, Entropy matters in grain boundary segregation, Acta Mater. 206 (2021) 116597, https://doi.org/10.1016/j.actamat.2020.116597.
[61] N. Tuchinda, C.A. Schuh, Computed entropy spectra for grain boundary segregation in polycrystals, NPJ. Comput. Mater. 10 (1) (2024) 72, https://doi.org/10.1038/s41524-024-01260-3.